Vibrational relaxation of N2 by collision with He atoms

A. J. Banks, D. C. Clary, and H.J. Werner

Citation: The Journal of Chemical Physics **84**, 3788 (1986); doi: 10.1063/1.450089
View online: http://dx.doi.org/10.1063/1.450089
View Table of Contents: http://scitation.aip.org/content/aip/journal/jcp/84/7?ver=pdfcov
Published by the AIP Publishing

Vibrational relaxation of N_2 by collision with He atoms

A. J. Banks, D. C. Clary, and H.-J. Werner[a)]
University Chemical Laboratory, Lensfield Rd., Cambridge CB2 1EW, United Kingdom

(Received 16 October 1985; accepted 18 November 1985)

A quantum mechanical study of vibrational relaxation in the collision of N_2 with ^3He and ^4He is reported. An *ab initio* potential energy surface has been computed using the coupled electron pair approximation with an extended basis set. Cross sections for $v = 1 \rightarrow 0$ vibrational relaxation have been calculated on this surface by using the centrifugal sudden approximation (CSA). The calculated vibrational relaxation rate coefficients show a very encouraging agreement with those measured in laser fluorescence experiments for the temperature range 82–291 K. Over this temperature range the rate coefficients increase by a factor close to 100. The CSA computations are also used to test the accuracy of the vibrational close coupling, rotational infinite order sudden, and the breathing sphere approximations.

I. INTRODUCTION

Many measurements of rate coefficients for vibrational energy transfer in gas phase atom–molecule collisions have been reported.[1] It is therefore surprising that few high quality calculations of such quantities have been performed. This is despite the fact that considerable progress has been made in recent years, both in the development of reliable and efficient *ab initio* methods to compute potential energy surfaces[2] and in the formulation and implementation of accurate scattering techniques capable of computing cross sections and rate coefficients for vibrational energy transfer from these potential surfaces.[3]

It is the purpose of this paper to report calculations of rate coefficients for the vibrational relaxation processes,

$$^4He + N_2(v = 1) \rightarrow {}^4He + N_2(v = 0),$$

$$^3He + N_2(v = 1) \rightarrow {}^3He + N_2(v = 0)$$

for temperatures below 300 K. We have used what are close to the best possible methods available to treat such a system theoretically. A full 3D potential energy function for the problem has been obtained as a fit to a large number of points on the $He + N_2$ surface calculated using the coupled electron pair approximation (CEPA-1)[4] with an extended basis set. In particular we allow the N_2 vibrational coordinate to vary in the *ab initio* calculations. The scattering dynamics are treated using the centrifugal sudden approximation (CSA)[5,6] which involves an explicit coupled channel calculation in both vibrational and rotational states of the N_2 molecule.

We compare our theoretical rate constants with those measured by Maricq *et al.* over the temperature range 82–291 K.[7] Over this range of temperatures, the rate coefficient for vibrational relaxation increases by a factor close to 100, and hence the experimental results present a particularly severe challenge to theory.

The CSA is expected to be a highly accurate method for vibrational relaxation in atom–diatomic molecule collisions as it has been tested by comparison with accurate close coupling results for $He + H_2$. In this case the CSA computations of vibrational relaxation cross sections were indistinguishable from the exact results.[8]

The CSA results for $He + N_2(v = 1 \rightarrow 0)$ have also been used to test the accuracy of more approximate methods. These include the vibrational close-coupling rotational infinite-order sudden approximation (VCC-IOSA), in which the close-coupled equations are solved for fixed atom–molecule orientation angles, and the breathing sphere approximation (BSA), in which only the isotropic part of the potential is used. These approximations have been extensively used in computations on vibrational relaxation in both diatomic[9–11] and polyatomic molecule collisions[12] but their accuracy remains uncertain. In the case of $He + H_2$, the VCC-IOSA vibrational relaxation cross sections are much lower than the accurate close-coupled results.[8] However, $He + H_2$ should be a particularly bad case for application of the VCC-IOSA as the rotational constant ($B_e = 60.8$ cm^{-1})[13] is so large that the application of the IOSA, in which the rotational levels are assumed to be degenerate, is highly questionable. Furthermore, the H_2 vibrational harmonic constant, $\omega_e = 4401.21$ cm^{-1}, is very high and thus the $He + H_2$ vibrational energy transfer is extremely inefficient and hence is highly sensitive to any dynamical approximations made in the calculations. In the case of $He + N_2$, the IOSA is expected to be more accurate than for $He + H_2$ as the molecular constants for N_2 are $B_e = 1.99824$ cm^{-1} and $\omega_e = 2358.57$ cm^{-1}. However, more accurate results are needed to test this assumption. In addition, we hope that our results will act as a benchmark for other approximate methods such as the semiclassical method of Billing[14] that have been widely used but have not yet been thoroughly tested on systems other than $He + H_2$.

The $He + N_2$ system has also been the subject of several recent comparisons between theory and experiment for rotational excitation.[15,16] It is rapidly becoming a benchmark atom–diatomic molecule system.

In Sec. II we describe our CEPA calculation of points on the $He + N_2$ potential energy surface and present details of the fit to the potential. Section III gives details of our CSA, VCC-IOSA, and BSA scattering computations and includes a discussion of the convergence tests applied to demonstrate

[a)] Permanent address: Institut für Physikalische und Theoretische Chemie, Johann Wolfgang Goethe Universität, D-6000 Frankfurt/M, West Germany.

 0021-9606/86/073788-10$02.10

the precision of the results. In Sec. IV calculations of vibrational relaxation cross sections and rate constants are presented and compared with the theoretical and experimental results. Conclusions are in Sec. V.

II. POTENTIAL ENERGY SURFACE

The strategy employed to generate the potential energy surface was to calculate points on the surface using highly correlated electronic wave functions. These points were then fitted to a suitable function in order to obtain an analytical expression for the potential which could be used in the scattering calculations.

The *ab initio* calculations were performed using the self-consistent electron pairs method (SCEP)[17,18] with the coupled electron pair approximation (CEPA-1).[4,17] This method was regarded as a good compromise between computational expense and accuracy. The SCEP-CEPA wave functions include explicitly all electron configurations which are singly or doubly excited relative to the SCF determinant and account for the most important effects of higher excited configurations approximately (the nitrogen 1*s* orbitals have not been correlated). It should be noted that the CEPA method is size extensive, i.e., the total energy for N_2 + He at a very large N_2–He distance equals exactly the sum of the individually calculated N_2 and He energies.

TABLE I. The CEPA *ab initio* interaction potential.[a]

		$\theta = 0.0°$	
R/a_0	r_1[b]	r_2	r_3
3.0	0.472 834(00)[c]	0.448 530(00)	0.513 699(00)
4.0	0.743 957(−1)	0.700 052(−1)	0.823 570(−1)
5.0	0.988 510(−2)	0.927 371(−2)	0.110 115(−1)
6.0	0.102 964(−2)	0.957 730(−3)	0.116 408(−2)
7.0	0.197 300(−4)	0.142 900(−4)	0.299 600(−4)
7.5	−0.385 600(−4)	−0.389 400(−4)	−0.374 100(−4)
8.0	−0.433 700(−4)	−0.425 900(−4)	−0.446 300(−4)
9.0	−0.261 200(−4)	−0.254 800(−4)	−0.274 400(−4)
10.0	−0.137 400(−4)	−0.133 300(−4)	−0.144 100(−4)
		$\theta = 45.0°$	
R/a_0	r_1	r_2	r_3
3.0	0.164 239(00)	0.162 234(00)	0.166 343(00)
4.0	0.283 790(−1)	0.273 808(−1)	0.299 313(−1)
5.0	0.371 344(−2)	0.355 064(−2)	0.398 259(−2)
6.0	0.299 450(−3)	0.280 760(−3)	0.333 520(−3)
7.0	−0.430 400(−4)	−0.434 500(−4)	−0.414 900(−4)
7.5	−0.494 700(−4)	−0.486 800(−4)	−0.502 900(−4)
8.0	−0.404 700(−4)	−0.395 000(−4)	−0.416 100(−4)
9.0	−0.216 500(−4)	−0.213 100(−4)	−0.223 700(−4)
10.0	−0.112 700(−4)	−0.110 300(−4)	−0.117 500(−4)
		$\theta = 90.0°$	
R/a_0	r_1	r_2	r_3
3.0	0.755 181(−1)	0.754 710(−1)	0.752 087(−1)
4.0	0.106 647(−1)	0.104 662(−1)	0.109 086(−1)
5.0	0.116 684(−2)	0.112 114(−2)	0.123 744(−2)
6.0	0.202 400(−4)	0.133 600(−4)	0.322 800(−4)
7.0	−0.536 600(−4)	−0.539 400(−4)	−0.527 300(−4)
7.5	−0.436 100(−4)	−0.433 800(−4)	−0.437 100(−4)
8.0	−0.323 100(−4)	−0.320 100(−4)	−0.327 100(−4)
9.0	−0.168 000(−4)	−0.164 900(−4)	−0.171 900(−4)
10.0	−0.896 000(−5)	−0.879 000(−5)	−0.914 000(−5)

[a] Energies are in hartree (E_h).
[b] $r_1 = 2.0744$, $r_2 = 2.0002$, $r_3 = 2.2000$.
[c] Numbers in parentheses are powers of 10.

A. *Ab initio* calculations

The CEPA calculations were carried out using the CRAY version of the SCEP program.[19] The potential was calculated for sets of R, r, and θ values, where R is the distance from the atom to the center of mass of the molecule, r is the internuclear separation in the nitrogen molecule, and θ is the angle between the vectors **R** and **r**. R took the values 3, 4, 5, 6, 7, 7.5, 8, 9, and 10 bohr with θ taking the values 0, 45, and 90 deg. The three r values chosen correspond to the maxima in the squared amplitudes of the N_2 ($v = 1$) vibrational wave function, $r_1 = 2.0002$ and $r_2 = 2.2$ bohr, and to the equilibrium bond distance, $r_e = 2.0744$ bohr.[13] A total of 81 points were thus calculated on the surface.

For the nitrogen atoms, the Huzinaga[20] 10*s*, 6*p* basis contracted to 6*s*, 4*p* (511111/3111) was used. Two *d*-function sets were added with exponents 0.95 and 0.2. For the helium atom, the Huzinaga 7*s* basis contracted to 5*s* (31111) and augmented by two *p*-functions with exponents 0.85 and 0.2 was used. The interaction energies were obtained by calculating the total and individual systems in the same basis set, i.e., basis set superposition errors were reduced by the usual counterpoise correction.[21] The results of the calculation are given in Table I.

To test the basis set and the quality of the electronic wave functions the interaction energies at some selected geometries were recalculated using more extensive basis sets. Furthermore, some properties of N_2 and He have been calculated. The interaction energies obtained with three different basis sets are shown in Table II. In this and the following tables basis I refers to the previously described basis set. Basis II is a more flexible basis set with 11*s*, 6*p*, 3*d* (7/5/3) for N_2 and 8*s*, 3*p* (6/3) for He which has been devised to obtain accurate dipole polarizabilities.[22] Basis III corresponds to basis I but included in addition an *f* function (exponent 0.25) on the nitrogen atoms and a *d* function (exponent 0.25) on the helium atom. These exponents were roughly optimized by maximizing their effect on the CEPA interaction energy at $R = 7.0$ bohr and $\theta = 90$ deg. It is noted that exponents which are optimized for the total energy are much

TABLE II. Calculated N_2–He interaction energies using CEPA-1 and various basis sets (see the text).

		CEPA interaction energy/E_h		
R/a_0[a]	Angle (θ)	Basis I	Basis II	Basis III
5.0	0.0	9.88(−3)[b]	9.71(−3)	9.58(−3)
8.0	0.0	−4.34(−5)	−4.38(−5)	−5.34(−5)
3.0	90.0	7.55(−2)	7.50(−2)	7.45(−2)
5.0	90.0	1.17(−3)	1.13(−3)	1.02(−3)
7.0	90.0	−5.36(−5)	−5.49(−5)	−6.85(−5)

[a] We set $r = 2.0744a_0$ in these calculations.
[b] Numbers in parentheses are powers of 10.

TABLE III. Calculated spectroscopic constants for N_2 (basis I).[a]

Method	r_e	B_e	α_e	ω_e	$\omega_e x_e$
SCF	1.070	2.102	0.0135	2730	11.0
CEPA-1	1.105	1.973	0.0164	2379	13.8
Expt.[b]	1.098	1.998	0.0173	2359	14.3

[a] r_e in Å, all other values in cm^{-1}.
[b] Reference 13.

larger, but the inclusion of such functions has only a very small effect on the interaction energies. Table II shows that the flexible functions in basis II have only a small effect on the results. More pronounced is the effect of the functions with higher angular momentum in basis III, particularly in the well region. However, in the repulsive part of the interaction potential their effect is quite small. Since the vibrational relaxation cross sections are expected to depend mainly on this part of the potential (except at very low temperatures), we decided to use the most cost effective basis I. Table III shows calculated spectroscopic constants for N_2 obtained with this basis. The theoretical equilibrium distance is 0.007 Å too long and the harmonic constant, ω_e, is 20 cm^{-1} too high. Such errors are typical for a basis set without f functions. The corresponding SCF errors for r_e and ω_e are -0.0275 Å and 372 cm^{-1}, respectively. In Table IV we present calculated static dipole polarizabilities and quadrupole moments for the three different basis sets. As expected, the polarizabilities obtained with basis I are 4%–5% too small. This error is reduced to less than 2% with basis III. The quadrupole moments obtained with basis sets II and III are 2%–3% larger than the value obtained with basis I. All polarizability values in Table IV have been evaluated at the experimental equilibrium distance since the vibrational correction for $v = 0$ is very small.[23] The quadrupole moments as a function of the internuclear distance have been calculated with basis I, and from this a vibrationally averaged CEPA value, $q_0 = -1.535(10^{-26})$esu cm^2 has been obtained. This result compares favorably with the recommended value $-1.52(10^{-26})$esu cm^2 of Stogryn and Stogryn.[24] Note that the SCF value is about 25% smaller. These results demonstrate the high quality of the CEPA wave functions.

TABLE IV. Calculated static dipole polarizabilities[a] and quadrupole moments[b] for N_2 and He.

	Basis	N_2 $\alpha_\parallel - \alpha_\perp$	N_2 $\bar{\alpha}$	N_2 q_e	N_2 q_0	He α
SCF	I	5.49	10.97	−1.21	−1.17	1.31
CEPA-1	I	4.66	11.25	−1.56	−1.54	1.38
	II	4.45	11.95	−1.60	−1.58[c]	1.38
	III	4.70	11.47	−1.61	−1.59[c]	1.39
Expt.		4.67	11.74		−1.52[d]	1.383

[a] Polarizabilities in a.u., evaluated as second derivative of the energy with respect to a finite electric field.
[b] Quadrupole moments in 10^{-26} esu cm^2.
[c] Zero point correction taken from CEPA value obtained with basis I.
[d] Recommended value of Stogryn and Stogryn (Ref. 24).

We note that canonical SCF orbitals have been employed in all CEPA calculations, which are not completely invariant with respect to unitary transformations among the occupied SCF orbitals. Localized orbitals might appear somewhat more suitable, but localization strongly degrades the convergence of the iterative SCEP-CEPA method. For some geometries we have compared the CEPA-1 and CEPA-2 approximations. The interaction energies differed by less than 2%.

For basis I the CRAY-1 CPU times required for one geometry with $\theta = 0$, 45, and 90 deg were 160, 260, and 130 s, respectively. A large part of this time was needed for the integral evaluation which is not vectorized. For 90 deg the times for individual steps were, e.g., 74s (integrals), 1.7s (SCF,N_2 + He, 10 iterations), and 20.0 s (CEPA,N_2 + He, 10 iterations, 17 228 CSFs).

B. Potential fit

The angularly and radially dependent potential is represented by the expansion

$$V(R,r,\theta) = \sum_{\lambda=0,1,2} \sum_{n=0,2,4} A_{n\lambda}(R) P_n(\cos\theta)(r - r_e)^\lambda, \quad (1)$$

where $P_n(\cos\theta)$ is a Legendre polynomial and the $A_{n\lambda}(R)$ are given by

TABLE V. Potential parameters, a_l^{mn} (in atomic units) for the least squares fit of Eq. (4) to the CEPA data.

l	$n=1$	$m=1$ $n=2$	$n=3$
1	0.135 796(3)[a]	0.101 673(3)	0.148 536(3)
2	0.146 001(1)	0.176 298(1)	0.144 325(1)
3	−0.308 214(0)	0.187 626(0)	−0.316 302(0)
4	0.328 422(−1)	−0.701 264(−1)	0.347 431(−1)
5	−0.121 125(−2)	0.450 044(−2)	−0.132 682(−2)
6	0.790 935(1)	0.806 979(1)	0.631 489(1)
7	0.518 476(3)	0.614 978(3)	0.658 915(3)
8	0.774 329(3)	−0.732 326(3)	0.114 849(4)
l	$n=1$	$m=2$ $n=2$	$n=3$
1	0.444 777(2)	0.112 729(3)	0.127 871(1)
2	0.135 504(1)	0.213 199(1)	0.179 756(1)
3	−0.337 846(0)	−0.481 436(0)	0.283 006(2)
4	0.394 809(−1)	0.236 797(0)	−0.606 547(1)
5	−0.160 701(−2)	−0.232 602(−1)	0.355 110(0)
6	0.605 134(1)	0.122 387(2)	0.748 212(1)
7	0.298 763(3)	−0.127 997(3)	0.486 879(3)
8	0.596 408(3)	0.235 037(4)	−0.735 326(3)
l	$n=1$	$m=3$ $n=2$	$n=3$
1	0.245 710(2)	0.174 902(2)	0.162 283(2)
2	0.150 062(1)	0.135 587(1)	0.172 696(1)
3	−0.289 025(0)	−0.360 724(0)	0.184 521(0)
4	0.281 702(−1)	0.451 181(−1)	−0.752 698(−1)
5	−0.864 732(−3)	−0.200 769(−2)	0.521 791(−2)
6	0.760 148(1)	0.663 149(1)	0.830 349(1)
7	0.191 659(3)	−0.387 097(2)	0.118 090(3)
8	−0.951 475(3)	0.124 073(3)	−0.691 299(3)

[a] Numbers in parentheses are powers of 10.

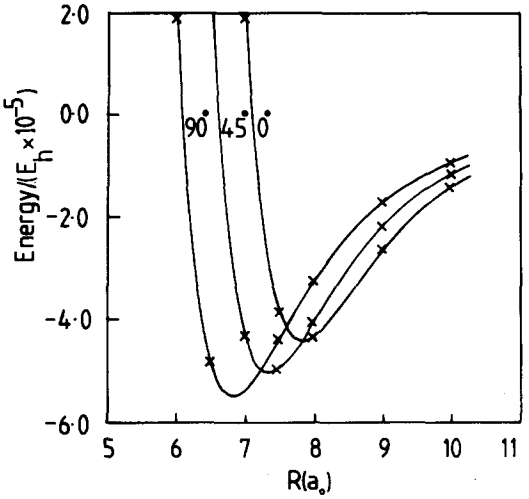

FIG. 1. A section of the elastic ($r=2.0744a_0$) CEPA interaction potential. The calculated points are marked by × and the solid line is the fit to the data.

$$A_{0\lambda}(R) = (1/105)[7B_{1\lambda}(R) + 56B_{2\lambda}(R) + 42B_{3\lambda}(R)],$$
$$A_{2\lambda}(R) = (2/105)[25B_{1\lambda}(R) + 20B_{2\lambda}(R) - 45B_{3\lambda}(R)], \quad (2)$$
$$A_{4\lambda}(R) = (16/105)[3B_{1\lambda}(R) - 6B_{2\lambda}(R) + 3B_{3\lambda}(R)],$$

where the numerical subscripts 1, 2, and 3 on the B coefficients denotes that the potential was evaluated with θ equal to 0°, 45°, and 90°, respectively. The B coefficients are given by the expressions

$$B_{m0} = b_{m1}(R),$$
$$B_{m1} = 2.957[1.865b_{m1}(R) - 2.865b_{m2}(R) + b_{m3}(R)], \quad (3)$$
$$B_{m2} = -39.849[2.693b_{m1}(R) - 1.693b_{m2}(R) - b_{m3}(R)],$$

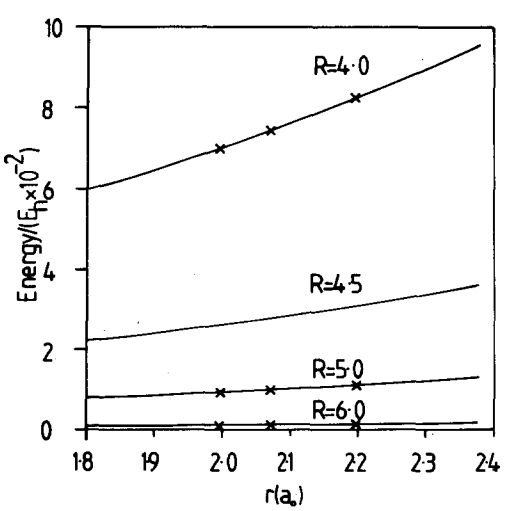

FIG. 2. The r dependence of the CEPA interaction potential for R values of 4, 4.5, 5, and 6 a_0 at $\theta = 0°$. The solid line is the fit to the calculated data denoted by ×.

TABLE VI. Test of potential expansion.

R	r	Angle(θ)	CEPA interaction energies[a]	
			calculated	fit
7.0	2.2	75	−5.371(−5)	−5.472(−5)
4.0	2.16	0.0	7.975(−2)	7.975(−2)

[a] R, r, and the energies are in atomic units, θ is in degrees.

where the numerical subscripts 1, 2, and 3 on the b coefficients now refer to the internuclear separation in the molecule being 2.0744, 2.0002, and 2.2000a_0, respectively. The individual $b_{mn}(R)$ functions are given by a least squares fit to the CEPA data of a function similar to that used by Huxley *et al.*[25] to represent the ground state potential of van der Waals diatomics,

$$b_{mn} = a_1^{mn}\exp(-a_2^{mn}R) \times (1 + a_3^{mn}R + a_4^{mn}R^2 + a_5^{mn}R^3) - \tanh(R)(a_6^{mn}/R^6 + a_7^{mn}/R^8 + a_8^{mn}/R^{10}). \quad (4)$$

The a_1^{mn} coefficients from the least squares fit are given in Table V, and a section of the resulting elastic potential (i.e., $r = 2.0744a_0$) for $\theta = 0°$, 45°, and 90° is shown in Fig. 1. An example of the r dependence of the potential for $\theta = 0°$ is shown in Fig. 2.

In order to test the potential expansion, comparisons of the fitted and calculated potential were made at angular and radial coordinates different from those used in the fitting. An example of such results is shown in Table VI and it can be seen that the error in the angular fit is less than 2% while that in the radial fit is less than 1%.

Table VII compares several potential energy surfaces about the well region.[16,26–28] For 0° the CEPA potential characteristics fall into the middle range of the other values. The CEPA potential shows less anisotropy as the 90° values indicate. In particular the well depth is more than a factor of 2 less than the HFD potentials, although better agreement is

TABLE VII. Comparison of elastic potential characteristics for various He–N_2 potentials.

Potential	$\epsilon(\theta)^a \times 10^5$		$R_m(\theta)^b$		$\sigma(\theta)^c$	
	0°	90°	0°	90°	0°	90°
CEPA	4.43	5.57	7.90	6.90	7.1	6.23
HFD1[d]	4.54	13.39	7.80	6.14	7.07	5.43
HFD2[d]	3.79	11.14	7.97	6.35	7.21	5.64
HTT[e]	3.87	8.98	8.00	6.71	7.35	5.95
KKM3[f]	6.25	10.27	8.02	6.80	7.06	5.98
KSK[g]	7.12	9.83	7.29	6.80	6.41	5.98

[a] ϵ is the depth of the potential well (a.u.).
[b] $R_m(\theta)$ is the position of the minimum of the well (a.u.).
[c] $\sigma(\theta)$ is the value of R at which $V(R,\theta) = 0.0$ (a.u.).
[d] Reference 16.
[e] Reference 26.
[f] Reference 28.
[g] Reference 27.

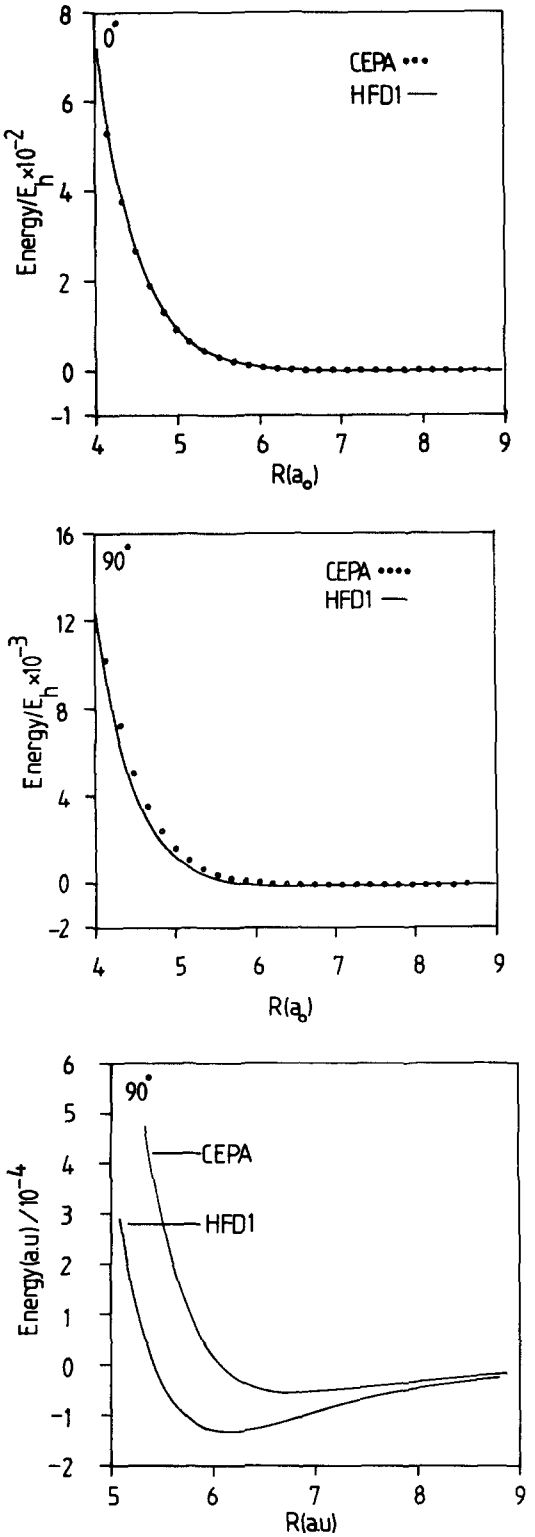

FIG. 3. Comparison of the CEPA potential and the HFD1 potential of McCourt *et al.* (Ref. 16) for 0° (3a), and 90° (3b). 3c compares the potentials at 90° in a region of lower energy.

found in the comparison with the KSK, KKM3, and HTT surfaces. Figure 3 shows a comparison of the CEPA potential and the HFD1 potential over a more extensive range than that considered in Table VII. The agreement at 0° remains very good over the range considered and the agreement between the potentials at 90° improves as the range, R, decreases. It is not surprising that the CEPA calculation with basis I yields a well depth which is too small. However, in view of the test calculations in Table II, we feel that an error of 100% in the well depth is unlikely, thus indicating that the anisotropy of the HFD1 potential is too large. From the point of view of vibrational relaxation in this system, the well depth should not be too important. The main feature of the potential which influences vibrational relaxation is the derivative of the potential with respect to the r coordinate at the classical turning point; thus it is important that the potential is accurate in the short range region.

A similar procedure was invoked to fit the SCF potential, with the b coefficients,

$$b_{mn} = a_1^{mn} \exp(-a_2^{mn} R)(1 + a_3^{mn} R + a_4^{mn} R^2 + a_5^{mn} R^3), \quad (5)$$

and the a_1^{mn} coefficients are given in Table VIII.

The potential energy surface for the nitrogen molecule was taken from Ref. 29, and was a function of the form

$$V(r) = -D_e[1 + c_1(r - r_e) + c_2(r - r_e)^2 + c_3(r - r_e)^3]\exp[-c_4(r - r_e)], \quad (6)$$

where r is the nitrogen internuclear distance, $D_e = 0.3640E_h$, $r_e = 2.0744a_0$, $c_1 = c_4 = 2.855a_0^{-1}$, $c_2 = 2.052a_0^{-2}$, and $c_3 = 0.739a_0^{-3}$.

III. SCATTERING CALCULATIONS

A. Theory

Calculations of vibrational relaxation cross sections and rate constants for $^4He(^3He) + N_2(v = 1 \rightarrow 0)$ were carried out using the CSA, VCC-IOSA, and BSA methods.

In the CSA we use body-fixed (BF) coordinates with the z axis along the atom–molecule center of mass vector $\mathbf{R}$.[6] The approximation[30]

TABLE VIII. Potential parameters, a_l^{mn}, (in atomic units) for the least squares fit of Eq. (5) to the SCF data.

		$m = 1$	
l	$n = 1$	$n = 2$	$n = 3$
1	0.894 625(−1)[a]	0.876 793(−1)	0.868 328(−1)
2	0.183 982(01)	0.184 823(01)	0.182 101(01)
3	0.955 826(03)	0.938 572(03)	0.103 344(04)
4	−0.196 293(03)	−0.190 934(03)	−0.216 080(03)
5	0.105 037(02)	0.101 208(02)	0.117 628(02)
		$m = 2$	
l	$n = 1$	$n = 2$	$n = 3$
1	−0.743 367(02)	0.507 461(−1)	0.479 654(−1)
2	0.194 474(01)	0.183 044(01)	0.180 197(01)
3	−0.104 338(01)	0.606 629(03)	0.627 225(03)
4	0.168 447(00)	−0.122 537(03)	−0.127 314(03)
5	−0.780 052(−2)	0.643 731(01)	0.672 374(01)
		$m = 3$	
l	$n = 1$	$n = 2$	$n = 3$
1	0.190 439(01)	0.149 921(01)	0.190 439(01)
2	0.194 802(01)	0.197 586(01)	0.194 802(01)
3	0.803 383(01)	0.110 122(02)	0.803 383(01)
4	−0.127 490(01)	−0.168 150(01)	−0.127 490(01)
5	0.502 183(−1)	0.618 623(−1)	0.502 183(−1)

[a] Numbers in parentheses are powers of 10.

$$|\mathbf{J}-\mathbf{j}|^2=\mathbf{J}^2+\mathbf{j}^2-2\mathbf{J}_z\mathbf{j}_z \tag{7}$$

is then made to the centrifugal term in the BF Hamiltonian. Here $\mathbf{J}$ is the total angular momentum and $\mathbf{j}$ the rotational angular momentum operator. The projection of $\mathbf{J}$ and $\mathbf{j}$ along the z axis is Ω. The coupled channel expansion

$$\psi^{J\Omega}=\sum_v\sum_j f_{vj}^{J\Omega}(R)\,g_{vj}^{\Omega}(r,\theta) \tag{8}$$

is used to obtain a set of coupled-channel equations for the translational functions $f_{vj}^{J\Omega}(R)$ which are solved using the R-matrix propagator method.[31,32] The vibrational–rotational basis functions $g_{vj}^{\Omega}(r,\theta)$ are obtained by diagonalizing the N_2 Hamiltonian utilizing the vibrational potential of Eq. (6). This was done by using the coupled basis set

$$h_v(r)\,Y_j^{\Omega}(\theta,0), \tag{9}$$

where $h_v(r)$ is a linear combination of harmonic oscillator basis functions which diagonalize the N_2 vibrational potential for $j=0$ and $Y_j^{\Omega}(\theta,0)$ is a spherical harmonic. The close-coupling matrix elements

$$\langle g_{vj}^{\Omega}(r,\theta)|V(R,r,\theta)|g_{v'j'}^{\Omega}(r,\theta)\rangle \tag{10}$$

are computed using Gauss–Hermite quadrature for r and analytical formulas involving Clebsch–Gordan coefficients for θ.[6]

Applications of boundary conditions yields the S-matrix elements $S_{v'j'\leftarrow vj}^{J\Omega}$ for the vibration–rotation transition $v'j'\leftarrow vj$. From these the vibrational relaxation cross sections are computed using the CSA expression

$$\sigma(vj\rightarrow v')=\pi/[k_{vj}^2(2j+1)]\times\sum_j\sum_J\sum_{\Omega}(2J+1)|S_{v'j'\leftarrow vj}^{J\Omega}|^2, \tag{11}$$

where $\hbar k_{vj}$ is the momentum for the initial vj state.

These calculations are repeated for a range of collision energies sufficient to give a rate coefficient $k(vj\rightarrow v')$ after Maxwell–Boltzmann averaging. Boltzmann averaging the j states of the $k(vj\rightarrow v')$ gives the rate coefficient $k(v\rightarrow v')$ which can be compared with the experimental measurements. In this Boltzmann averaging the even–odd j states are weighted 2:1 in accordance with the nuclear spin statistics.

In the VCC-IOSA calculations the approximations $|\mathbf{J}-\mathbf{j}|^2=\hbar^2J(J+1)$ and $\mathbf{j}^2=0$ are made. It is then necessary to use the coupled channel expression

$$\psi^J=\sum_v f_v^J(R;\theta)h_v(r) \tag{12}$$

for a range of angles, θ. The angle dependent S-matrix elements obtained by applying boundary conditions are $S_{v'\leftarrow v}^J(\theta)$. From these the VCC-IOSA vibrational relaxation cross sections,

$$\sigma(v\rightarrow v')=(\pi/2k_v^2)\sum_J(2J+1)\times\int_0^{\pi}\sin\theta\,d\theta\,|S_{v'\leftarrow v}^J(\theta)|^2 \tag{13}$$

can be computed.

In the BSA, the approximation $|\mathbf{J}-\mathbf{j}|^2=\hbar^2J(J+1)$ is employed and only the isotropic part of the potential is used. The coupled-channel expansion

$$\psi^J=\sum_v f_v^J(R)h_v(r) \tag{14}$$

is then employed and the S-matrix elements are $S_{v'\leftarrow v}^J$. The BSA vibrational cross sections are

$$\sigma(v\rightarrow v')=(\pi/k_v^2)\sum_J(2J+1)|S_{v'\leftarrow v}^J|^2. \tag{15}$$

B. Numerical details

This section gives details of the parameters which set the numerical accuracy of the scattering calculations.

Sixteen primitive harmonic oscillator functions were used to generate the nitrogen vibrational wave functions and energies. The wave functions were calculated at 24 points for use in the Gauss–Hermite evaluation of the matrix elements.

Because nitrogen is a homonuclear diatomic, odd and even rotational states can be considered independently, only needing to be brought together at the final statistically weighted Boltzmann averaging. This effectively halves the size of the basis set required, making the computation much more tractable than similar problems involving heteronuclear diatomics. Table IX shows the results of calculations of the cross sections $\sigma(v=1,j\rightarrow v'=0)$ over a range of energies (with J held to a maximum value of 15 to conserve CPU time) for a selection of basis sets. It can be seen that the 15,16,6 basis set used in the calculations gives cross sections converged to within 1% even for the highest rotational state used. Here (j_0,j_1,j_2) refers to the basis set in which j_i represents the number of rotational basis functions in vibrational state i. Thus $j_0=15$ corresponds to a maximum j value of 28 in $v=0$.

A convergence test in the program allowed the summation over J to continue until only a 1% increase in the cross section with increasing J was obtained. Doubling the stringency of this test caused less than a 0.5% rise in the cross section. For the propagation routine, 120 equally spaced sectors between 3 and $25a_0$ gave cross sections converged to within 2%.

Cross sections, $\sigma(v=1,j\rightarrow v=0)$, were calculated for at least 7 energies with Ω values up to 18 considered. The j dependent rate constants were calculated by fitting the natu-

TABLE IX. Details of basis set convergence tests for the CSA calculations.

Basis set[a]	Cross sections/a_0^2		
	$j=0$	$j=10$	$j=18$
13,12,6	7.51(−7)[b]	7.81(−7)	4.78(−9)
15,12,6	7.51(−7)	7.75(−7)	4.86(−9)
17,12,6	7.51(−7)	7.75(−7)	4.89(−9)
15,14,7	7.49(−7)	7.67(−6)	3.86(−9)
15,16,6	7.49(−7)	7.66(−7)	3.74(−9)
15,18,6	7.49(−7)	7.66(−7)	3.74(−9)

[a] The cross sections were calculated with $\Omega=0$ and no degeneracy averaging. J was allowed a maximum value of 15. The translational energies for the above cross sections were $E_{trans}^{vj}=0.1$, 0.0731, and 0.0162 eV for $j=0$, 10, and 18, respectively. The notation for the basis set (m,n,l) is explained in the text.

[b] Numbers in parentheses are powers of 10.

TABLE X. Cross sections (in a_0^2,) $\sigma(v=1,j=0\rightarrow v'=0)$, for $^4He + N_2(v=1\rightarrow 0)$ calculated using the CEPA potential.

Energy (eV)	CSA($j=0$)	VCC-IOSA	BSA	CSA/VCC-IOSA
0.0119	2.96(−9)[a]	3.58(−10)	1.65(−10)	8.3
0.0336	2.52(−8)	4.40(−9)	2.06(−9)	5.7
0.0881	6.85(−7)	1.73(−7)	8.29(−8)	3.9
0.115	2.17(−6)	5.80(−7)	2.80(−7)	3.7
0.2	2.59(−5)	8.56(−6)	4.24(−6)	3.0
0.3	1.70(−4)	6.73(−5)	3.19(−5)	2.5
0.4	6.74(−4)	2.91(−4)	1.06(−4)	2.3

[a] Numbers in parentheses are powers of 10.

ral logarithm of the cross section, $\sigma(vj\rightarrow v')$, to a cubic spline function and interpolating to give sufficient points for a Simpson's rule integration over energy. The initial j dependent rate constant was Boltzmann averaged to give the final vibrational relaxation rate constant. A total of 18 j states were used in the Boltzmann average and this was sufficient to give a room temperature rate constant converged to within 1%. To carry out a CSA calculation at one energy using the 15,16,6 basis, summing over 18 Ω values and obtaining convergence at $J=30$ required 1137 s of CRAY I CPU time.

IV. RESULTS AND DISCUSSION

Tables X and XI present a comparison of the CSA cross sections, $\sigma(v=1,j=0\rightarrow v'=0)$, with the VCC-IOSA and BSA cross sections for $^4He + N_2$ and $^3He + N_2$, respectively. For ^4He the ratio CSA/VCC-IOSA decreases from 8.27 at the translational energy $E^{vj}_{trans}=0.0119$ eV to 2.31 at 0.4 eV. Thus the accuracy of the VCC-IOSA does improve considerably as the energy increases. It is interesting to note that the VCC-IOSA results are more accurate for ^3He, where the cross sections are close to an order of magnitude larger, than those for ^4He. The BSA cross sections are roughly a factor of 2 lower than the IOSA. The reason underlying the rather disappointing accuracy of the VCC-IOSA cross sections at lower energies is related to the very low values of the cross sections, and their extreme sensitivity to translational energy. Simple theories[33] suggest that vibrational relaxation cross sections are exponentially dependent on the energy gap between vibrational levels. Rotational excitation in the $v=0$ state will reduce the effective energy gap and help to increase the efficiency of the vibrational relaxation. Rotational energies are not explicitly included in the VCC-IOSA. Examination of the final j state dependence of $\sigma(v=1,j\rightarrow v'=0,j')$ shows a distribution which tends to peak around $j'=16$. This behavior reflects the balance between angular momentum conservation and energy gap effects.

TABLE XI. Cross sections (in a_0^2), $\sigma(v=1,j=0\rightarrow v'=0)$, for $^3He + N_2(v=1\rightarrow 0)$ calculated using the CEPA potential.

Energy (eV)	CSA($j=0$)	VCC-IOSA	BSA	CSA/VCC-IOSA
0.0119	3.89(−8)[a]	7.31(−9)	4.68(−9)	5.3
0.0336	2.50(−7)	6.39(−8)	4.13(−8)	3.9
0.0881	4.38(−6)	1.53(−6)	1.03(−6)	2.9
0.1	6.91(−6)	2.52(−6)	1.69(−6)	2.7
0.2	1.01(−4)	4.66(−5)	3.19(−5)	2.2
0.3	4.83(−4)	2.77(−4)	1.92(−4)	1.7
0.4	1.58(−3)	9.87(−4)	6.91(−4)	1.6

[a] Numbers in parentheses are powers of 10.

TABLE XII. Rate constants (in units of $cm^3\,s^{-1}$ molecule^{-1}) for $^4He + N_2(v=1\rightarrow 0)$ calculated using the CEPA potential.

T(K)	Experimental[a]	CSA	CSA($j=0$)	VCC-IOSA
291	5.1 ± 0.1 (−18)[b]	4.29(−18)	2.61(−18)	7.57(−19)
262	3.2 ± 0.1 (−18)	2.65(−18)	1.58(−18)	4.35(−19)
210	1.1 ± 0.05(−18)	9.87(−19)	5.68(−19)	1.40(−19)
175	5.0 ± 0.3 (−19)	4.56(−19)	2.54(−19)	5.73(−20)
156	3.3 ± 0.3 (−19)	2.88(−19)	1.57(−19)	3.34(−20)
149	2.7 ± 0.2 (−19)	2.41(−19)	1.30(−19)	2.71(−20)
132	1.6 ± 0.15(−19)	1.52(−19)	8.01(−20)	1.58(−20)
100	3.2 ± 1.5 (−20)	5.57(−20)	2.92(−20)	5.08(−21)

[a] Reference 7.
[b] Numbers in parentheses are powers of 10.

The CSA vibrational relaxation rate coefficients, Boltzmann averaged over j, $k(v=1\rightarrow 0)$ are given in Table XII and illustrated in Fig. 4 for the $^4He + N_2$ system. Also shown are the experimental[7] VCC-IOSA, BSA, and CSA ($j=0$) [i.e., $k(v=1,j=0\rightarrow v'=0)$] rate coefficients. The CSA calculation is within 20% of the experimental value at room temperature and this agreement improves to 5% at lower temperatures, with the exception of the experimental point at the lowest temperature. The CSA ($j=0$) results are a factor of 3 higher than the VCC-IOSA results at room temperature. The difference increases as the temperature decreases. The BSA rate coefficients are a factor of 2 lower than the VCC-IOSA results throughout the temperature range, these trends reflecting those in the cross sections. The rate constants for different initial j values, $k(v=1j\rightarrow v'=0)$, are shown in Fig. 5 and a significant "j effect" can be seen. It is this effect which is responsible for

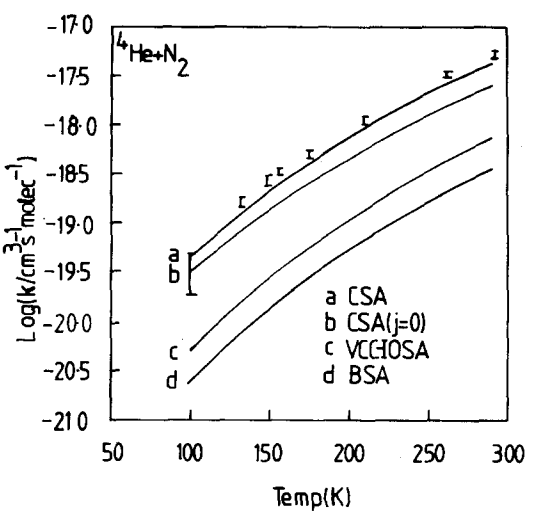

FIG. 4. The rate coefficients $k(v=1\rightarrow 0)$ for $^4He + N_2$ calculated using the CEPA potential. The error bars give the experimental results (Ref. 7). CSA refers to the j averaged $k(v=1,j\rightarrow v'=0)$ and CSA$(j=0)$ to $k(v=1,j=0\rightarrow v'=0)$.

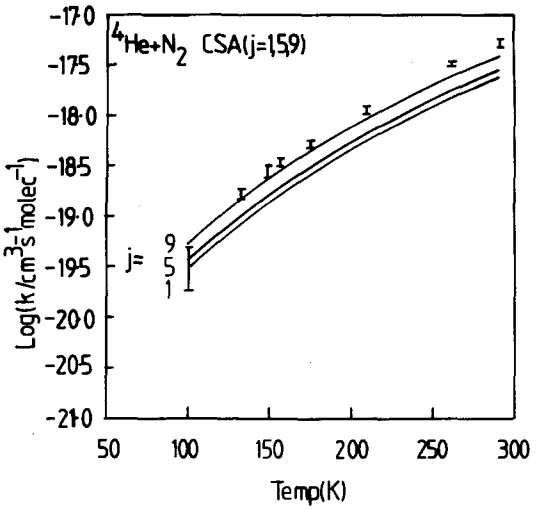

FIG. 5. The initial j dependence of CSA rate coefficients, $k(v=1,j\rightarrow v'=0)$, for $^4He + N_2(v=1)$ calculated using the CEPA potential. The error bars denote the experimental results (Ref. 7).

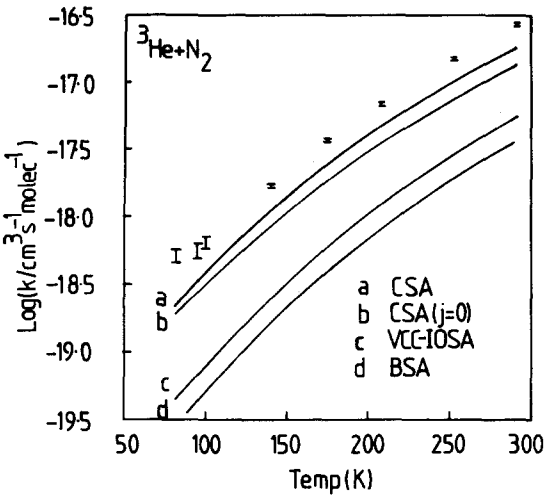

FIG. 7. The rate coefficients $k(v=1\rightarrow 0)$ for $^3He + N_2$ calculated using the CEPA potential. The error bars give the experimental results (Ref. 7). CSA refers to the j averaged $k(v=1,j\rightarrow v'=0)$ and CSA$(j=0)$ to $k(v=1,j=0\rightarrow v'=0)$.

the greater value of the rate constant obtained from the full CSA calculation as compared to that from the CSA$(j=0)$ calculation. The reason for this effect is the coupling of rotational and translational motion which serves to increase the effective translational energy giving rise to larger cross sections.

Figure 6 shows the CSA$(j=0)$ rate constants for both the CEPA and the SCF potential. The SCF potential gives rate constants that are a factor of 2 lower than those calculated from the CEPA potential at room temperature, the difference increasing with decreasing temperature to give a factor of 3 difference at 100 K. Two possible reasons are suggested for this phenomena. Firstly, the absence of a well in the SCF potential will be important at lower temperatures. Secondly, the radial dependence of the SCF and CEPA potentials is similar for a given R and θ value with the SCF potential shifted to a higher energy due to the lack of electron correlation. This, coupled with the fact that the steepness of the radial dependence drops as R increases (see Fig. 2) implies that for a given energy a steeper r dependence is experienced on the CEPA surface.

Figure 7 and Table XIII give the rate coefficients calculated for $^3He + N_2$. The experimental/CSA rate coefficient ratio is 1.46 at room temperature. The VCC-IOSA rate constants are a factor of between 2 and 4 lower than the CSA$(j=0)$ rate constants over the temperature range 291–82 K, with the BSA calculations giving results a factor of 2 lower than the VCC-IOSA calculations. The initial j dependent rate constants are illustrated in Fig. 8. It can be seen that the j effect is less dramatic for ^3He than for ^4He.

Overall the agreement between the CSA results and experiments is very encouraging. The vibrational relaxation rate constants increase by a factor close to 100 over the temperature range considered, yet the CSA results agree to within a factor of 2 with experiment for ^3He and within 20% for ^4He. Furthermore, the calculations have been performed using an *ab initio* potential with no parameters adjusted to fit extra types of data such as the long range part of the potential. Our results are purely *ab initio* predictions.

It is likely that the remaining discrepancies between theory and experiment are due to the potential energy surface

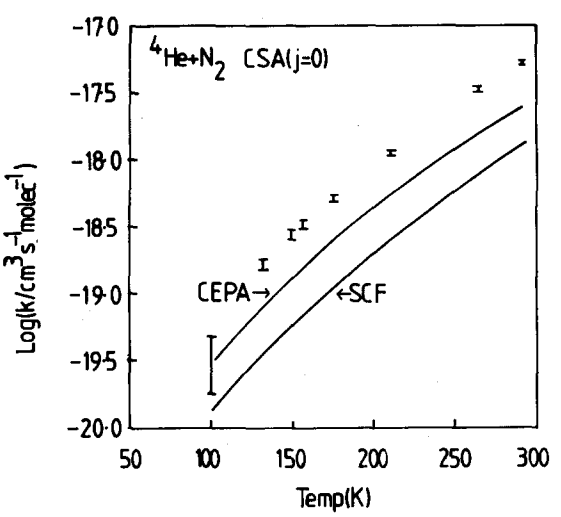

FIG. 6 The CSA$(j=0)$,$k(v=1,j=0\rightarrow v'=0)$ rate coefficients calculated using the CEPA and SCF potentials for the $^4He + N_2(v=1)$ system. The error bars denote experimental results (Ref. 7).

TABLE XIII. Rate constants (in units of cm^3 s^{-1} molecule^{-1}) for $^3He + N_2(v=1\rightarrow 0)$ calculated using the CEPA potential.

T(K)	Experimental[a]	CSA	CSA$(j=0)$	VCC-IOSA
291	2.7 ± 0.04 (− 17)[b]	1.85(− 17)	1.38(− 17)	5.56(− 18)
252	1.5 ± 0.04 (− 17)	1.03(− 17)	7.62(− 18)	2.89(− 18)
207	6.9 ± 0.15 (− 18)	4.68(− 18)	3.47(− 18)	1.21(− 18)
174	3.7 ± 0.1 (− 18)	2.42(− 18)	1.80(− 18)	5.86(− 19)
140	1.7 ± 0.08 (− 18)	1.12(− 18)	8.39(− 19)	2.49(− 19)
100	6.2 ± 0.6 (− 19)	3.79(− 19)	3.05(− 19)	7.75(− 20)
95	5.3 ± 0.5 (− 19)	3.26(− 19)	2.67(− 19)	6.61(− 20)
82	5.0 ± 0.5 (− 19)	2.16(− 19)	1.88(− 19)	4.36(− 20)

[a] Reference 7.
[b] Numbers in parentheses are powers of 10.

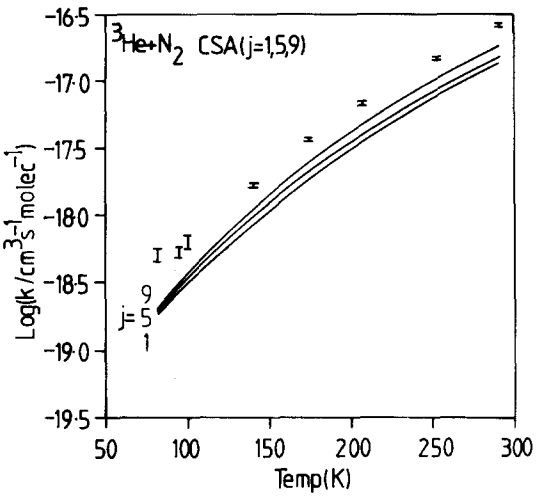

FIG. 8. The initial j dependence of CSA rate coefficients $k(v=1,j\rightarrow v'=0)$, for ^{3}He + $N_2(v=1)$ calculated using the CEPA potential. The error bars denote the experimental results (Ref. 7).

used in the calculation. Table II shows that the addition of an f function on the nitrogen atom and a d function on the helium atom to the basis set used in computing the potential energy surface gives a slight increase in the depth of the potential well. This implies that the potential we used will be slightly too repulsive. If the potential was made more attractive, then the scattering atom would be able to reach regions of the potential where the vibrational coupling is stronger (see Fig. 2) and the vibrational rate constants would increase.

It is interesting to compare these results with the recent calculations of Schinke *et al.* on $H_2 + CO(v=1)$[34] and He + $CO(v=1)$[35] and also with the comparison of the VCC-IOSA and semiclassical CSA calculations of Price *et al.* for He + $CO(v=1)$.[11] The CSA/VCC-IOSA ratio of cross sections in He + N_2 is larger than that reported for He, H_2 + CO. This is related to the smaller and therefore more sensitive cross sections for He + N_2. The fact that, due to the homonuclear symmetry, nonzero rotational transitions in N_2 must involve at least a change of 2 in the rotational quantum number may also be important as this effectively doubles the rotational constant. The increase in the CSA/VCC-IOSA ratio with increasing energy, as found for ^{3}He + CO,[35] was not found for ^{3}He + N_2. The ratio $k_{CSA}/k_{CSA(j=0)}$ for ^{4}He + N_2 lies between the 1.1–1.2 estimated for H_2 + CO[34] and the factor of 2–4 found in the comparison of VCC-IOSA and semiclassical CSA for He + CO.[11] We find a minimum ratio of 1.1 for ^{3}He at 82 K and a maximum ratio of 1.9 for ^{4}He at 100 K.

Clearly the validity of the VCC-IOSA approximation is very much dependent on the collisional system, the potential, the masses of the atoms involved, the vibrational frequency, and the sensitivity of the cross sections to collision energy. For molecules, such as nitrogen, with large vibrational frequencies, the method must be used with great care. We note that the VCC-IOSA has been used to parametrize a potential to fit the experimental rate constant data for He + N_2.[7] Our results suggest that this is a questionable procedure for systems such as this.

V. CONCLUSION

Quantum mechanical calculations on the $v=1\rightarrow 0$ vibrational relaxation of N_2 in collision with ^{4}He and ^{3}He have been reported. The method involves a CEPA calculation of points on the He + N_2 potential energy surface, a functional fit to these points and a CSA calculation of cross sections for vibrational relaxation.

Our *ab initio* calculations of rate constants give a very encouraging comparison with experimental results previously reported for temperatures below 300 K.[7] The CSA results have also been used to test the accuracy of more approximate theories—the VCC-IOSA and BSA. Although the VCC-IOSA vibrational relaxation cross sections do improve in accuracy considerably as the collisional energy is increased, the rate coefficients fall well below the CSA results for the temperature range considered. This is attributed to the very small magnitude of the cross sections which are sensitive to effects such as rotational levels reducing the effective energy gap between the vibrational levels. We also find that the vibrational relaxation cross sections and rate coefficients increase as the initial rotational state is increased. It is therefore important to perform the full Boltzmann average over the initial rotational states when calculating the vibrational relaxation rate coefficients.

We emphasize here that the He-N_2 system should not be considered as a prototype system for all vibrational energy transfer problems. In particular, polyatomic energy transfer has been the subject of intense study[1] and these molecules have vibrational modes of much lower frequency than N_2 and thus display more efficient energy transfer making the cross sections less sensitive to rotational effects.[36] The VCC-IOSA should, therefore, be more reliable for many polyatomic molecule collisions.[12]

In the case of atom–diatom systems, however, the He + N_2 system is rapidly becoming a benchmark collisional system, from the point of view of elastic,[37] rotational,[15,16] and vibrational energy transfer and other properties.[16] It is thus important to attempt to compute a set of accurate results for this system which will enable us to test the accuracy of approximate techniques of calculation and even check the reliability of experiments.

The current study shows that if state-of-the-art methods are used, both to calculate the potential energy surface and to treat the scattering dynamics, then an encouraging agreement with experiment can be obtained for vibrational relaxation in He + N_2. For this and similar systems, it is clear that more approximate methods of calculation cannot be relied upon to give results of quantitative accuracy.

ACKNOWLEDGMENTS

This work was supported by the Science and Engineering Research Council and the EEC. HJW acknowledges support by the Fonds der Chemischen Industrie and Deutsche Forschungsgemeinschaft. The calculations were performed on the CRAY-15 computer at the University of London Computer Centre.

[1]R. T. Bailey and F. R. Cruickshank, in *Gas Kinetics and Energy Transfer*, edited by P. G. Ashmore and R. J. Donovan (The Chemical Society, London, 1978), p. 109.
[2]*Advanced Theories and Computational Approaches to the Electronic Structure of Molecules*, edited by C. E. Dykstra (Reidel, Dordrecht, 1984).
[3]D. G. Truhlar, Int. J. Quantum Chem. Symp. **17**, 77 (1983).
[4]W. Meyer, Int. J. Quantum Chem. Symp. **5**, 341 (1971); J. Chem. Phys. **58**, 1017 (1973).
[5]P. McGuire and D. J. Kouri, J. Chem. Phys. **60**, 2488 (1974).
[6]R. T Pack, J. Chem. Phys. **60**, 633 (1974).
[7]M. M. Maricq, E. A. Gregory, C. T. Wickham-Jones, D. J. Cartwright, and C. J. S. M. Simpson, Chem. Phys. **75**, 347 (1983).
[8]D. R. Flower and D. J. Kirkpatrick, J. Phys. B **15**, 1701 (1982).
[9]J. M. Bowman and S. C. Leasure, J. Chem. Phys. **66**, 288 (1977).
[10]R. Schinke and P. McGuire, Chem. Phys. **31**, 391 (1978).
[11]R. J. Price, D. C. Clary, and G. D. Billing, Chem. Phys. Lett. **101**, 269 (1983).
[12]D. C. Clary, J. Chem. Phys. **75**, 209 (1981); J. Am. Chem. Soc. **106**, 970 (1984).
[13]K. P. Huber and G. Herzberg, *Molecular Spectra and Structure, Vol. 4, Constants of Diatomic Molecules* (Van Nostrand, New York, 1979).
[14]G. D. Billing, Chem. Phys. **33**, 227 (1978).
[15]M. Faubel, K.-H. Kohl, J. P. Toennies, K. T. Tang, and Y. Y. Yung, J. Chem. Soc. Faraday Discuss. **73**, 205 (1982).
[16]F. R. McCourt, R. R. Fuchs, and A. J. Thakkar, J. Chem. Phys. **80**, 5561 (1984); R. R. Fuchs, F. R. W. McCourt, A. J. Thakkar, and F. Grein, J. Phys. Chem. **88**, 2036 (1984).
[17]W. Meyer, J. Chem. Phys. **64**, 2901 (1976).
[18]H.-J. Werner and E. -A. Reinsch, J. Chem. Phys. **76**, 3144 (1982).
[19]H. -J. Werner and E. -A. Reinsch, in *Advanced Theories and Computational Approaches to the Electronic Structure of Molecules*, edited by C. E. Dykstra, (Reidel, Dordrecht, 1984), p. 79.
[20]S. Huzinaga, J. Chem. Phys. **42**, 1293 (1965).
[21]S. F. Boys and F. Bernardi, Mol. Phys. **19**, 553 (1970).
[22]H. -J. Werner and W. Meyer, Mol. Phys. **31**, 855 (1976).
[23]W. Meyer, P. Botschwina, P. Rosmus, and H. -J. Werner, in *Computational Methods in Chemistry*, edited by J. Bargon (Plenum, New York, 1980), p. 157.
[24]D. E. Stogryn and A. P. Stogryn, Mol. Phys. **11**, 371 (1966).
[25]P. Huxley, D. B. Knowles, J. N. Murrell, and J. D. Watts, J. Chem. Soc. Faraday Trans. 2 **80**, 1349 (1984).
[26]P. Habitz, K. T. Tang, and J. P. Toennies, Chem. Phys. Lett. **85**, 461 (1982).
[27]M. Keil, J. T. Slankas, and A. Kuppermann, J. Chem. Phys. **70**, 541 (1979).
[28]W. -K. Liu, F. R. McCourt, D. E. Fitz, and D. J. Kouri, J. Chem. Phys. **75**, 1496 (1981).
[29]P. Huxley and J. N. Murrell, J. Chem. Soc. Faraday Trans. 2 **79**, 323 (1983).
[30]G. C. Schatz and A. Kuppermann, J. Chem. Phys. **65**, 4668 (1976).
[31]J. C. Light and R. B. Walker, J. Chem. Phys. **65**, 4272 (1976).
[32]E. B. Stechel, R. B. Walker, and J. C. Light, J. Chem. Phys. **69**, 3518 (1978).
[33]J. T. Yardley, *Introduction to Molecular Energy Transfer* (Academic, New York, 1980).
[34]Z.Bačić, R. Schinke, and G. H. F. Diercksen, J. Chem. Phys. **82**, 236, 245 (1985).
[35]R. Schinke and G. H. F. Diercksen, J. Chem. Phys. **83**, 4516 (1985).
[36]D. C. Clary, J. Chem. Phys. **81**, 4466 (1984).
[37]R. Candori, F. Pirani, F. Vecchiocattivi, F. A. Gianturco, U. T. Lamanna, and G. Petrella, Chem. Phys. **92**, 345 (1985).